# Quantum teleportation of physical qubits into logical code spaces

Yi-Han Luo[a,b,c,1], Ming-Cheng Chen[a,b,c,1], Manuel Erhard[d,e,1], Han-Sen Zhong[a,b,c], Dian Wu[a,b,c], Hao-Yang Tang[a,b,c], Qi Zhao[a,b,c], Xi-Lin Wang[a,b,c], Keisuke Fujii[f], Li Li[a,b,c], Nai-Le Liu[a,b,c], Kae Nemoto[g,h], William J. Munro[g,h], Chao-Yang Lu[a,b,c,2], Anton Zeilinger[d,e,2], and Jian-Wei Pan[a,b,c,2]

[a]Hefei National Laboratory for Physical Sciences at Microscale, University of Science and Technology of China, Hefei 230026, China; [b]Department of Modern Physics, University of Science and Technology of China, Hefei 230026, China; [c]Chinese Academy of Sciences Centre for Excellence and Synergetic Innovation Centre in Quantum Information and Quantum Physics, Hefei, Anhui 230026, China; [d]Institute for Quantum Optics and Quantum Information, Austrian Academy of Sciences, A-1090 Vienna, Austria; [e]Vienna Center for Quantum Science and Technology, Faculty of Physics, University of Vienna, A-1090 Vienna, Austria; [f]Division of Advanced Electronics and Optical Science, Graduate School of Engineering Science, Osaka University, Toyonaka 560-8531, Japan; [g]NTT Basic Research Laboratories, NTT Research Center for Theoretical Quantum Physics, NTT Corporation, Kanagawa 243-0198, Japan; and [h]National Institute of Informatics, Tokyo 101-8430, Japan

Contributed by Anton Zeilinger, July 6, 2021 (sent for review January 2, 2021; reviewed by Hugues de Riedmatten and Fabio Sciarrino)

**Quantum error correction is an essential tool for reliably performing tasks for processing quantum information on a large scale. However, integration into quantum circuits to achieve these tasks is problematic when one realizes that nontransverse operations, which are essential for universal quantum computation, lead to the spread of errors. Quantum gate teleportation has been proposed as an elegant solution for this. Here, one replaces these fragile, nontransverse inline gates with the generation of specific, highly entangled offline resource states that can be teleported into the circuit to implement the nontransverse gate. As the first important step, we create a maximally entangled state between a physical and an error-correctable logical qubit and use it as a teleportation resource. We then demonstrate the teleportation of quantum information encoded on the physical qubit into the error-corrected logical qubit with fidelities up to 0.786. Our scheme can be designed to be fully fault tolerant so that it can be used in future large-scale quantum technologies.**

quantum computing | quantum error correction | quantum teleportation | quantum entanglement

It is well known that quantum mechanics provides a new paradigm for the creation, manipulation, and transmission of information in ways that exceed conventional approaches (1, 2). These tasks, whether they be in computation, communication, or metrology, are generally represented by some form of quantum circuit. As the size of these circuits increases, noise and imperfections in the fundamental quantum gates used to implement those circuits render them unreliable to perform the tasks one wanted to do (3). The natural solution is quantum error correction schemes which allow one to construct logical qubits resilient to those errors (4–7). With logical operations, one can then undertake large-scale quantum information tasks. It is essential that, as part of this, one needs to be able to get "data" in and out of the processor in a reliable fashion.

Quantum error correction works by encoding the information that is present on a single qubit into a logical qubit, a special type of highly entangled state. This logical qubit has the property that certain errors move the state out of the code space holding the logical qubit (8). One can then use ancillary qubits to detect and correct those errors in a nondemolition way (5–10). By increasing the redundancy in the degree of freedom within the logical qubit, the errors can be suppressed to arbitrarily low levels. When the physical error rate is below a certain threshold, it is possible to avoid errors propagating through the circuit to ensure the reliable quantum computation—a concept known as fault tolerance (3–5). It is the key to large-scale quantum information processing tasks which generally take a form illustrated in Fig. 1*A*. Here a single qubit holding initial quantum information is encoded into a logical block with the encoding circuit which includes the physical qubits required by quantum error correction code (QECC) and additional ancillary qubits used for the error detection and correction. The encoded logical block is then directed to further logical operation in a fault-tolerant manner. One immediately notices that we have separated these into transversal and nontransversal gates. The transversal gates have the essential property of preventing error propagation between physical qubits inside QECC (11). Any QECC requires both transversal and nontransversal gates for universal quantum computation. Typically, most Clifford gates are transversal, and their fault-tolerant implementation is straightforward, whereas non-Clifford gates such as the T ($\pi/8$) gate are nontransversal, and hence the realization of a logical T ($\pi/8$) gate is the key for universal quantum computation.

Through the introduction of quantum teleportation (12), these difficulties with nontransversal gates can be addressed. Here we employ a maximally entangled Bell state of the form

$$|\Phi^+\rangle = \frac{1}{\sqrt{2}}(|0\rangle|0\rangle_{\mathrm{L}} + |1\rangle|1\rangle_{\mathrm{L}}), \qquad [1]$$

where the subscript L denotes the logical QECC protected state space. As shown in Fig. 1*C*, the teleportation utilizes a Bell

## Significance

**Quantum teleportation and quantum error correction play crucial roles in fault-tolerant quantum computing. Here, we implemented error-correctable quantum teleportation to manipulate a logical qubit and observed the protection of quantum information. Our work presents a useful technology for scalable quantum computing and can serve as a quantum simulator for holographic quantum gravity.**

Author contributions: M.-C.C., C.-Y.L., A.Z., and J.-W.P. designed research; Y.-H.L., M.-C.C., M.E., H.-S.Z., D.W., H.-Y.T., Q.Z., X.-L.W., L.L., and C.-Y.L. performed research; N.-L.L. contributed new reagents/analytic tools; Y.-H.L., M.-C.C., M.E., H.-S.Z., D.W., H.-Y.T., Q.Z., X.-L.W., K.F., L.L., K.N., W.J.M., C.-Y.L., and J.-W.P. analyzed data; and Y.-H.L., M.-C.C., M.E., H.-S.Z., D.W., H.-Y.T., Q.Z., X.-L.W., K.F., L.L., N.-L.L., K.N., W.J.M., C.-Y.L., A.Z., and J.-W.P. wrote the paper.

Reviewers: H.d.R., Institute of Photonic Sciences; and F.S., Universita degli Studi di Roma La Sapienza.

The authors declare no competing interest.



[1]Y.-H.L., M.-C.C., and M.E. contributed equally to this work.

[2]To whom correspondence may be addressed. Email: cylu@ustc.edu.cn, anton.zeilinger@univie.ac.at, or pan@ustc.edu.cn.

This article contains supporting information online at https://www.pnas.org/lookup/suppl/doi:10.1073/pnas.2026250118/-/DCSupplemental.

Published September 3, 2021.

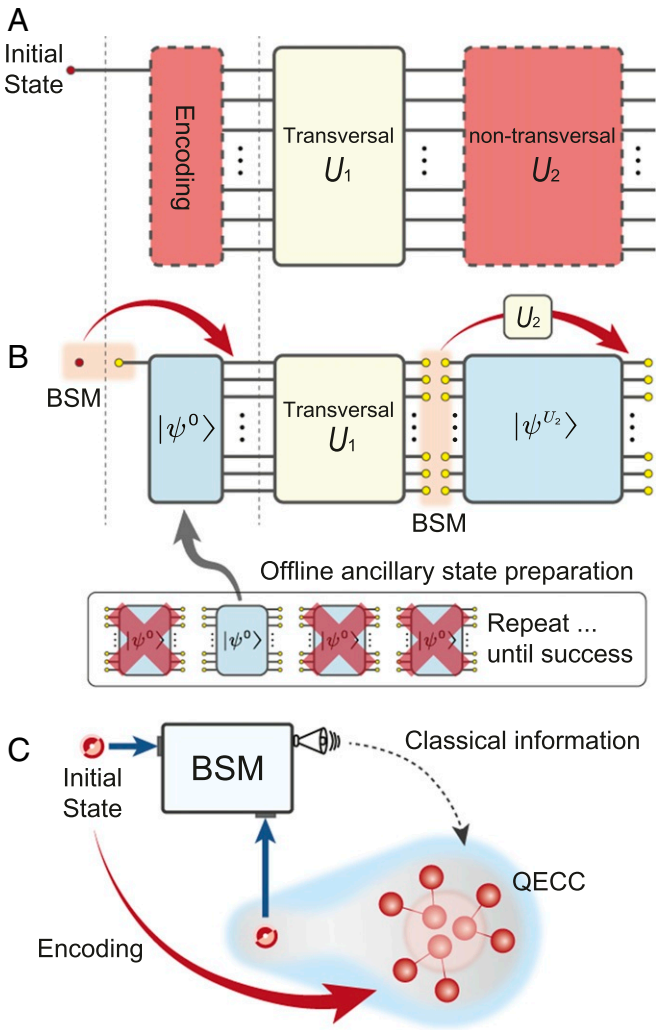


**Fig. 1.** Schematic illustration of teleportation-based error correction state encoding. In *A* and *B*, we show the fault-tolerant quantum circuit before and after combining with quantum teleportation, where the unreliable operations, unknown state encoding, and nontransversal gate $U_2$ are marked with red blocks. The flow of quantum information is transmitted along the circuit from left to right. In *A*, errors will be accumulated as the number of unreliable operations grows. In contrast, by introducing quantum teleportation, the "fragile nodes" can be replaced with preestablished entanglement states taking a specific form. As shown in *B*, the encoding process and nontransversal gate $U_2$ are replaced with states $|\psi^0\rangle$ and $|\psi^{U_2}\rangle$. Upon encountering "fragile nodes," such as encoding, the circuit is paused until a suitable $|\psi^0\rangle = |\Phi^+\rangle$ is generated. Then the BSM transforms quantum information holding by the initial state into the QECC, which can then be further operated by following logical gates. Scheme in *C* illustrates the teleportation-based QECC encoding where, to encode the unknown initial state, a physical qubit is entangled with logical qubit encoded in a specific QECC. Then the BSM is performed between initial qubit and the physical qubit with the measurement results fed forward to complete the transfer of our quantum information into the QECC.

state measurement (BSM) between the initial state $|\psi\rangle$ to be teleported and the single physical qubit of $|\Phi^+\rangle$. Classical feedforward of our BSM result ensures the initial quantum state is teleported into the encoded qubit. All these procedures, including the generation of $|\Phi^+\rangle$ together with BSM, can, in principle, be performed in a fault-tolerant manner (2). Quantum teleportation allows us to perform nontransversal gates offline, where the probabilistic gate preparation can be done, as shown in Fig. 1*B*. The initial state $|\psi\rangle$ could be an arbitrary state; however, the choice of the state $|A\rangle = (|0\rangle + e^{i\pi/4}|1\rangle)/\sqrt{2}$, known as a magic state, is the most relevant to quantum computation. It is used to implement the $T$ gate through magic state injection (3, 13)—a crucial approach toward a fault-tolerant non-Clifford gate. The same mechanism holds for a fault-tolerant implementation of nontransversal gates when the offline state preparation achieves the required precision through repeat-until-success strategies. More generally, a recursive application of this protocol allows us to implement a certain class of gates fault tolerantly, including a Toffoli gate (14), which is also indicated in Fig. 1*B*. It is equally important to note that the quantum teleportation to the logical qubit is an important building block for distributed quantum computation and global quantum communications. The teleportation-based quantum error correction schemes thus have the potential to significantly lower the technical barriers in our pursuit of larger-scale quantum information processing (QIP).

In stark contrast to theoretical progress, quantum teleportation and QECC have been developed independently in the experimental regime. We have seen quite a number of remarkable quantum teleportation demonstrations (15–27) and QECC experiments (28–35) performed in a number of physical systems. However, the experimental combination of these operations, quantum teleportation-based quantum error correction, is still to be realized. Given that it is an essential tool for future larger-scale quantum tasks, it will be our focus here.

In this work, we report on an experimental realization of the teleportation of information encoded on a physical qubit into an error-protected logical qubit. This is a key step in the development of quantum teleportation-based error correction. We begin by establishing an Einstein–Podolsky–Rosen channel—the entangled resource state for an error-protected logical qubit. Quantum teleportation involving a physical qubit of the entangled resource state transfers the quantum information encoded in one single qubit into the error-protected logical qubit. The quality of the entanglement resource state and the performance of the quantum teleportation are then evaluated.

## Experimental Implementation

The scheme shown in Fig. 1*B* is conceptually very similar to the original teleportation protocol; however, currently, it is significantly more challenging due to the necessity of creating the entangled resource Eq. **1** involving a logical encoded qubit—especially when one considers optical implementations. Here our logical qubit basis states

$$|0\rangle_{\mathrm{L}} = \frac{1}{2\sqrt{2}}(|000\rangle + |111\rangle)^{\otimes 3},$$
$$|1\rangle_{\mathrm{L}} = \frac{1}{2\sqrt{2}}(|000\rangle - |111\rangle)^{\otimes 3} \qquad [2]$$

are associated with the (9,1,3) Shor code (2), which is a repetition of the three-photon Greenberger–Horne–Zeilinger ($\mathrm{GHZ}_3$) state (36). More details concerning Shor code can be found in *SI Appendix*. Now, given the complexity here, it is crucial to design and configure our optical circuit efficiently, remembering that, in linear optical systems, most multiple-qubit gates are probabilistic (but heralded) in nature. Only gates including the controlled NOT (CNOT) gate between different degrees of freedom (DOFs) on the same single photon can be implemented in a deterministic fashion.

Our experiment is divided into three key stages: 1) the creation of the entangled resource state $|\Phi^+\rangle$; 2) the preparation and teleportation of the initial physical qubit $|\varphi\rangle$ into the logical qubit $|\varphi\rangle_L$; and 3) readout of the logical state $|\varphi\rangle_L$ and detection of error syndromes.

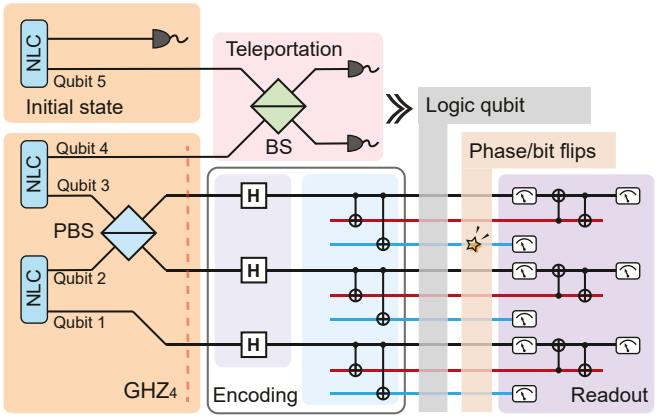


**Fig. 2.** Principle experimental scheme. We employ three nonlinear crystals (NLCs) to create six photons in total. Two NLCs in combination with a PBS create a $GHZ_4$ state in the polarization DoF. The fifth photon is programmed with an arbitrary qubit state $|\varphi\rangle$ to be teleported, while the sixth photon serves as a trigger. Shown in the green box is a beam splitter (BS) in combination with coincidence detection to implement the BSM necessary to teleport the quantum state $|\varphi\rangle$ of the fifth photon into the QECC space. The readout stage (purple box) used to measure the error syndromes contains three consecutive measurement stages. First, the path DoF is measured, followed by the polarization DoF. Finally, the OAM DoF is measured using an OAM-to-polarization converter. This, in total, results in eight single-photon detectors (SPDs) per photon, and thus 24 SPDs for the logic qubit readout stage only.

The first key stage is the creation of the $|\Phi^+\rangle$ state performed using the quantum circuit shown in Fig. 2. It begins by generating a polarization-entangled four-photon GHZ ($GHZ_4$) state (36) using beam-like type-II spontaneous parametric down-conversion (SPDC) in a sandwich-like geometry (37). This particular geometry produces a maximally entangled two-photon state, and so, in order to create a $GHZ_4$ state, photons 2 and 3 are combined on a polarizing beam splitter (PBS), which transmits horizontally ($H$) polarized photons and reflects vertically (V) polarized photons. A fourfold coincidence registration detects the four photons in the GHZ state $|\psi^4\rangle = (|H\rangle^{\otimes 4} + |V\rangle^{\otimes 4})/\sqrt{2}$. Among these four photons, photon 4 acts as the physical qubit to be used in the BSM, while photons 1, 2, and 3 are directed to the logical qubit encoding circuit. Now, to construct the nine-qubit Shor code with three photons, we use two more DoFs per photon associated with the path and orbital angular momentum (OAM). Using additional DoFs is not only resource efficient in terms of the number of photons required but also enables us to use deterministic CNOT gates using linear optical elements only (see *SI Appendix* for details).

Experimentally, the creation of the Shor code (Fig. 2) begins by applying Hadamard gates on the polarization DoF of each photon using a half-wave plate (HWP) at 22.5°. This transforms the GHZ state to

$$|\psi'^4\rangle = (|H\rangle|+\rangle^{\otimes 3} + |V\rangle|-\rangle^{\otimes 3})/\sqrt{2}, \qquad [3]$$

where $|\pm\rangle = (|H\rangle \pm |V\rangle)/\sqrt{2}$ and $|-\rangle = (|H\rangle - |V\rangle)/\sqrt{2}$ denote the diagonal and antidiagonal polarization, respectively. The other DoFs are initially in their $|0\rangle$ state. Then two consecutive CNOT gates are applied, where the polarization always acts as the control, and the other two DoFs act as the target qubits. With the control qubit $|\pm\rangle$ and target qubits $|0\rangle$, a three-qubit GHZ state $|0,0,0\rangle \pm |1,1,1\rangle$ is generated on each photon. We have thus generated the desired 10-qubit physical–logical QECC entangled state $|\Phi^+\rangle = (|H\rangle|0\rangle_L + |V\rangle|1\rangle_L)/\sqrt{2}$, ending the first stage.

The second stage of the experiment concerns the teleportation of the state $|\varphi\rangle = \alpha|H\rangle + \beta|V\rangle$ on its own independent physical qubit into the QECC protected logical qubit, as depicted in Fig.1*B*. Here we use a photon (photon 5) prepared in a separate $\beta$-barium borate (BBO) crystal (heralded by the second photon of the pair) to encode an arbitrary single-qubit state into the polarization DoF using half- and quarter-wave plates. A BSM to implement the teleportation is carried out with a 50/50 beam splitter and subsequent coincidence measurement on that polarization encoded qubit and the physical qubit from the entangled resource $|\Phi^+\rangle$. Usually, this method projects the two photons onto the antisymmetric Bell state $|\psi^-\rangle$; however, by transforming the state before the beam splitter using HWPs, we project onto the symmetrical $(|HH\rangle + |VV\rangle)/\sqrt{2}$ state (38), which, ideally, results in the following logical state:

$$|\varphi\rangle_L = \alpha|0\rangle_L + \beta|1\rangle_L. \qquad [4]$$

The third and final part of the experiment consists of the logical state's $|\varphi\rangle_L$ readout and error syndromes detection. Ideally, one should use ancilla qubits to measure the error syndromes and use those results to correct any errors before measuring the state of the logical qubit. This would require extra photons and active feed-forward correction techniques. Instead, here we post-select on results that lie within the error-protected code space; see ref. 30 as an example. As displayed in Fig. 2, a bit flip of one of the nine physical qubits encoding the logical qubit $|\varphi\rangle_L$ results in a change of the error syndrome measurements (see *SI Appendix*) and thus can be excluded. The Shor code can also detect phase flips or linear combinations of bit and phase flips that form arbitrary unitary transformations.

Finally, we can independently measure and read out each DoF for photons 1, 2, and 3 without disturbing or destroying the quantum information encoded in the other DoFs (39). In our experiment, the DoFs of polarization, paths, and OAM are measured step by step. The qubit encoded with polarization and paths is directly read out with standard polarization analyzers and Mach–Zehnder interferometers. For the OAM encoded qubit, a swap gate is used to transfer the OAM state to a polarization one where it can be measured with another polarization analyzer. These measurements give us access to the complete logical qubit, consisting of three photons in three different DoFs, and access to the complete Shor code space of nine physical qubits. Further details are described in *SI Appendix*.

## Experimental Results

The crucial ingredient for our experiment is the generation of the maximally entangled quantum state between the physical and logical qubit. It is important to first evaluate the quality of this entangled resource state. Typical quantum state tomography on 10 qubits is unfeasible due to the number of measurements involved. However, the code structure allows us to eliminate this daunting task to evaluate it at the physical level. The logical level evaluation perfectly serves our purpose, and so we instead measure the state fidelity and the Clauser–Horne–Shimony–Holt (CHSH) inequality to evaluate the entanglement between the logical and physical qubits. The density matrix of $|\Phi^+\rangle$ can be expressed as

$$\rho = \frac{1}{4}(I \otimes I_{cs} + X \otimes X_L^{cs} - Y \otimes Y_L^{cs} + Z \otimes Z_L^{cs}), \qquad [5]$$

involving the usual Pauli operators for the physical and logical qubit. Measuring the fidelity is equivalent to determining the expectation values of all four observables above, requiring $4 \times 2^8 = 1{,}024$ settings in total. Fortunately, the expectation values of the Pauli matrices $I$, $Z$ can be obtained with equal settings.

Further owing to special features of the Shor code stabilizers, the number of settings can be further reduced to 250 in total (see *SI Appendix*). For each setting, we record fourfold coincidences for 10 s, yielding a coincidence rate of $\sim 150\ \mathrm{s}^{-1}$. We obtain a fidelity for the ideal state $|\Phi^+\rangle$ as $F = 0.703(2)$. This clearly surpasses the genuine entanglement 0.5 threshold. However, this fidelity $F$ is insufficient to violate a CHSH inequality with $\langle \mathrm{CHSH} \rangle = 1.974(3) < 2$ experimental determined. Detailed measurement results for the estimation of the fidelity and CHSH inequality are shown in Fig. 3.

Next, we exclude the influence of correctable errors by confining the state of the logical qubit to the actual code space using the projectors $I_{\mathrm{cs}}$ to the code space (see *SI Appendix* for details). Experimentally, the overlap results in $\langle I \otimes I_{\mathrm{cs}} \rangle = 0.808(2)$, representing the overlap between the logic qubit prepared in our experiment and the code space. This is then used to exclude all errors that can be detected by the stabilizers, yielding an error-corrected state fidelity $F = 0.870(3)$ and $\langle \mathrm{CHSH} \rangle = 2.443(3) > 2$ violation within the code space (Fig. 3). Furthermore, the encoded state fidelity $F = 0.870 > 0.85$ would enable magic state distillation with error-corrected Clifford gates. Our results clearly demonstrate the effectiveness of QECC in our approach, but unity fidelity was not achieved, due to multipair emissions and nonfactorizable joint spectral amplitudes within the SPDC process utilized for generating the $|\Phi^+\rangle$ state. Such errors cannot be corrected by our encoding, as they sit inside the code space (see *SI Appendix* for details).

With the entangled resource state characterized, we now need to explore the operation of teleporting a physical qubit into the logical qubit space. For such a quantum system, it is necessary to show its performance, comprehensively exceeding any classical methods. Thus, in our experiment, we select eigenstates with eigenvalue $+1$ of three Pauli matrices $X$, $Y$, and $Z$, denoted as $|0\rangle$, $|+\rangle$, and $|R\rangle$, respectively, and measure their teleported fidelity. We measure 125 settings for $|0\rangle, |R\rangle$ and 98 settings for $|+\rangle$. For each setting, we accumulate, on average, $\sim$60 coincidences in 1,200 s, which corresponds to a count rate of $\sim 0.05$ Hz. The achieved experimental fidelities (with and without correction) and the projection probabilities $I_{\mathrm{cs}}$ are shown in Fig. 4.

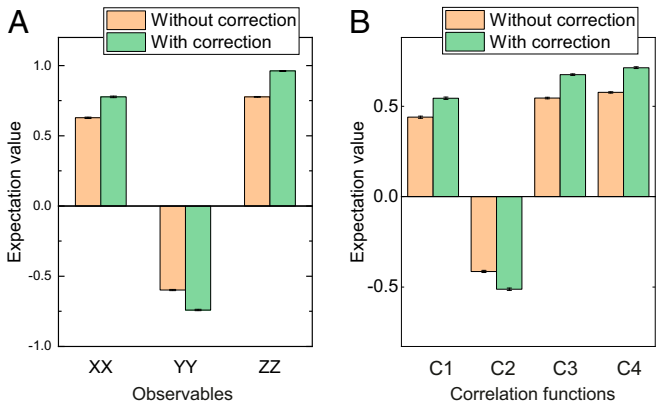


**Fig. 3.** Characterization of the entanglement teleportation resource state. In *A*, we show the measured expectation values of $X \otimes X_{\mathrm{L}}$, $Y \otimes Y_{\mathrm{L}}$, and $Z \otimes Z_{\mathrm{L}}$ without (orange bars) and with (green bars) correction. One can determine the fidelity of entangled state as $F = 0.703(2)$ before and $F = 0.870(3)$ after correction. Similarly, *B* shows the measured correlation functions required for the CHSH inequality without (orange bars) and with (green bars) error correction. The physical qubit is measured in the $E_{1,2} = (Z \pm X)/\sqrt{2}$ basis, while the QEEC is measured with $X_{\mathrm{L}}, Z_{\mathrm{L}}$, respectively. The four correlation functions $C_1, C_2, C_3$, and $C_4$ denote $E_1 \otimes X_{\mathrm{L}}$, $E_2 \otimes X_{\mathrm{L}}$, $E_1 \otimes Z_{\mathrm{L}}$, and $E_2 \otimes Z_{\mathrm{L}}$, respectively. Then $\langle \mathrm{CHSH} \rangle = C_1 - C_2 + C_3 + C_4$ gives 1.974(3) before and 2.443(3) after correction. All reported measurements are without background or accidental count subtraction, while the stated measurement errors are obtained using Monte Carlo simulation with an underlying Poissonian distribution of photon counting statistics.

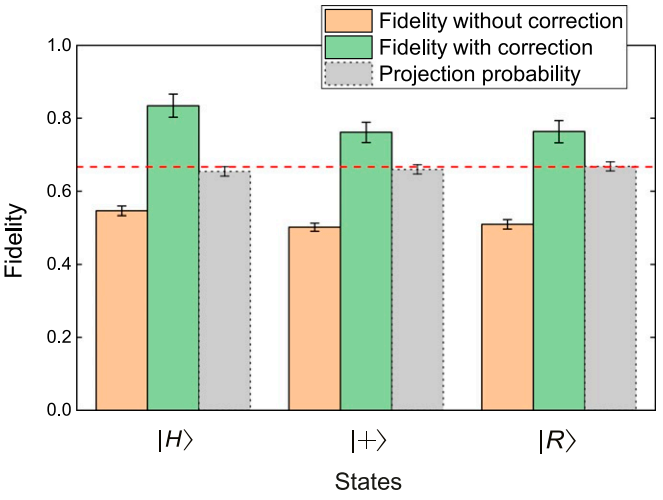


**Fig. 4.** Experimental teleportation of an arbitrary single-qubit state. Here we show the teleportation results of three representative states $|H\rangle$, $|+\rangle$, and $|R\rangle$ that are eigenstates of $\sigma_z$, $\sigma_x$, anb $\sigma_y$, respectively, with eigenvalue $+1$. For each state, the fidelity with and without correction is shown together with the projection probability. After correction, the averaged fidelity of the three teleported states is 0.786(17), well exceeding the 2/3 classical limit shown as a red dashed line.

The averaged fidelity of the three logic states is $0.520(7)$, while, after projection into the code space, it increases to $0.786(17)$. This is well above the classical limit of $2/3$. Furthermore, in our experimental arrangements, the teleportation fidelity of any state of the form $(|0\rangle + e^{i\phi}|1\rangle)/\sqrt{2}$ is independent of the phase $\phi$. For example, the fidelities of $\phi = 0$ and $\phi = \pi/2$ are consistent in 1 SD, as shown in Fig. 4. The obtained results demonstrate the ability of our approach to write via quantum teleportation arbitrary quantum states, including the magic state $\phi = \pi/4$ for $T$ gate, from a single physical qubit into the logical code space consisting of nine physical qubits. Moreover, the postselected error correction scheme employed here significantly increases the observed average fidelities from $\sim 52$ to $\sim 78\%$ limited only by noncorrectable errors stemming from multipair emissions of the SPDC processes.

## Discussion and Conclusion

In summary, we have demonstrated the teleportation of a physical qubit into a logical qubit formed from a QECC. This is a key step for optical quantum calculation on a larger scale. Although the results achieved are far from the fault tolerance threshold, our work is still far reaching. It demonstrates the ability to introduce well-developed quantum teleportation to the QIP at the logical level within current technology, and, as such, represents a crucial step toward fault-tolerant QIP. Such an ability is essential for probabilistic gate operations to be performed on an unknown state in a scalable manner. More specifically and importantly, it allows for magic state injection, a critical task in error-corrected quantum computation. Our experiment can be further modified to adapt the fault-tolerant manner. Moreover, within the theoretical scheme, it can be further concatenated with independently developed modules, such as magic state distillation and transversal logical operation block, that may become a useful part of future implementations of fault-tolerant quantum computer. For a global quantum internet based on optical fibers, it will be necessary to employ quantum repeaters to overcome the intrinsic losses in the optical fibers. To distribute quantum entan-

glement in such a network, QECC is potentially necessary. In this sense, our presented scheme could be useful in a future quantum internet.

In addition, the demonstrated quantum entanglement between a physical qubit and a logical qubit is a versatile building block for many novel quantum information tasks. It enables a teleportation-based divide-and-conquer method to realize deep-depth quantum computing similar to the strategy used in long-distance quantum communication, which is exponentially resource efficient (40). It is also a basic structure to simulate quantum gravity. The quantum correlation between the central physical qubit and the logical qubit in the boundary is an implementation of the holographic principle, which is the basic rule to understand the space–time structure in quantum gravity from the view of quantum entanglement (41). Our high-fidelity transport of quantum state between the bulk and boundary qubits demonstrates a kind of holographic equivalence.

**Data Availability.** All study data are included in the article and *SI Appendix*.

**ACKNOWLEDGMENTS.** This work was supported by the National Natural Science Foundation of China; the Chinese Academy of Sciences; the National Fundamental Research Program; the Anhui Initiative in Quantum Information Technologies; Ministry of Education, Culture, Sports, Science and Technology Quantum Leap Flagship Program Grant JPMXS0118069605; the Austrian Federal Ministry of Education, Science and Research; and the University of Vienna via the project Quantum Experiments on Space Scale.

1. A. G. J. MacFarlane, J. P. Dowling, G. J. Milburn , Quantum technology: The second quantum revolution. *Philos. Trans. A Math. Phys. Eng. Sci.* **361**, 1655–1674 (2003).
2. M. A. Nielsen, I. L. Chuang, *Quantum Computation and Quantum Information: 10th Anniversary Edition* (Cambridge University Press, ed. 10, 2011).
3. E. Knill, Quantum computing with realistically noisy devices. *Nature* **434**, 39–44 (2005).
4. P. W. Shor, "Fault-tolerant quantum computation"in *Proceedings of the 37th Annual Symposium on Foundations of Computer Science* (IEEE Computer Society, 1996), p. 56.
5. D. Gottesman, Theory of fault-tolerant quantum computation. *Phys. Rev. A* **57**, 127–137 (1998).
6. C. H. Bennett, D. P. DiVincenzo, J. A. Smolin, W. K. Wootters, Mixed-state entanglement and quantum error correction. *Phys. Rev. A* **54**, 3824–3851 (1996).
7. S. J. Devitt, W. J. Munro, K. Nemoto, Quantum error correction for beginners. *Rep. Prog. Phys.* **76**, 076001 (2013).
8. P. W. Shor, Scheme for reducing decoherence in quantum computer memory. *Phys. Rev. A* **52**, R2493–R2496 (1995).
9. A. M. Steane, Error correcting codes in quantum theory. *Phys. Rev. Lett.* **77**, 793–797 (1996).
10. R. Laflamme, C. Miquel, J. P. Paz, W. H. Zurek, Perfect quantum error correcting code. *Phys. Rev. Lett.* **77**, 198–201 (1996).
11. B. Eastin, E. Knill, Restrictions on transversal encoded quantum gate sets. *Phys. Rev. Lett.* **102**, 110502 (2009).
12. C. H. Bennett *et al*., Teleporting an unknown quantum state via dual classical and Einstein-Podolsky-Rosen channels. *Phys. Rev. Lett.* **70**, 1895–1899 (1993).
13. A. G. Fowler, M. Mariantoni, J. M. Martinis, A. N. Cleland, Surface codes: Towards practical large-scale quantum computation. *Phys. Rev. A* **86**, 032324 (2012).
14. D. Gottesman, I. Chuang, Demonstrating the viability of universal quantum computation using teleportation and single-qubit operations. *Nature* **402**, 390–393 (1999).
15. D. Bouwmeester *et al*., Experimental quantum teleportation. *Nature* **390**, 575–579 (1997).
16. A. Furusawa *et al*., Unconditional quantum teleportation. *Science* **282**, 706–709 (1998).
17. I. Marcikic, H. de Riedmatten, W. Tittel, H. Zbinden, N. Gisin, Long-distance teleportation of qubits at telecommunication wavelengths. *Nature* **421**, 509–513 (2003).
18. Q. Zhang *et al*., Experimental quantum teleportation of a two-qubit composite system. *Nat. Phys.* **2**, 678–682 (2006).
19. X. L. Wang *et al*., Quantum teleportation of multiple degrees of freedom of a single photon. *Nature* **518**, 516–519 (2015).
20. J. G. Ren *et al*., Ground-to-satellite quantum teleportation. *Nature* **549**, 70–73 (2017).
21. Y. H. Luo *et al*., Quantum teleportation in high dimensions. *Phys. Rev. Lett.* **123**, 070505 (2019).
22. G. Carvacho *et al*., Experimental study of nonclassical teleportation beyond average fidelity. *Phys. Rev. Lett.* **121**, 140501 (2018).
23. X. H. Bao *et al*., Quantum teleportation between remote atomic-ensemble quantum memories. *Proc. Natl. Acad. Sci. U.S.A.* **109**, 20347–20351 (2012).
24. M. Riebe *et al*., Deterministic quantum teleportation with atoms. *Nature* **429**, 734–737 (2004).
25. M. D. Barrett *et al*., Deterministic quantum teleportation of atomic qubits. *Nature* **429**, 737–739 (2004).
26. W. Pfaff *et al*., Quantum information. Unconditional quantum teleportation between distant solid-state quantum bits. *Science* **345**, 532–535 (2014).
27. L. Steffen *et al*., Deterministic quantum teleportation with feed-forward in a solid state system. *Nature* **500**, 319–322 (2013).
28. C. Y. Lu *et al*., Experimental quantum coding against qubit loss error. *Proc. Natl. Acad. Sci. U.S.A.* **105**, 11050–11054 (2008).
29. X. C. Yao *et al*., Experimental demonstration of topological error correction. *Nature* **482**, 489–494 (2012).
30. D. Nigg *et al*., Quantum computations on a topologically encoded qubit. *Science* **345**, 302–305 (2014).
31. J. Chiaverini *et al*., Realization of quantum error correction. *Nature* **432**, 602–605 (2004).
32. P. Schindler *et al*., Experimental repetitive quantum error correction. *Science* **332**, 1059–1061 (2011).
33. M. D. Reed *et al*., Realization of three-qubit quantum error correction with superconducting circuits. *Nature* **482**, 382–385 (2012).
34. J. Kelly *et al*., State preservation by repetitive error detection in a superconducting quantum circuit. *Nature* **519**, 66–69 (2015).
35. N. Ofek *et al*., Extending the lifetime of a quantum bit with error correction in superconducting circuits. *Nature* **536**, 441–445 (2016).
36. D. Greenberger, M. Horne, A. Shimony, A. Zeilinger, Bell theorem without inequalities. *Am. J. Phys.* **58**, 1131–1143 (1990).
37. X. L. Wang *et al*., Experimental ten-photon entanglement. *Phys. Rev. Lett.* **117**, 210502 (2016).
38. J. W. Pan *et al*., Multiphoton entanglement and interferometry. *Rev. Mod. Phys.* **84**, 777 (2012).
39. X. L. Wang *et al*., 18-qubit entanglement with six photons' three degrees of freedom. *Phys. Rev. Lett.* **120**, 260502 (2018).
40. L. M. Duan, M. D. Lukin, J. I. Cirac, P. Zoller, Long-distance quantum communication with atomic ensembles and linear optics. *Nature* **414**, 413–418 (2001).
41. X. L. Qi, Does gravity come from quantum information? *Nat. Phys.* **14**, 984–987 (2018).